Synthesis, Structural, Density Functional Theory, and X-Ray Diffraction Study of Zn(II) *N*-Isopropylbenzyldithiocarbamate: Anti-Corrosion Screening in Acid Media

Noor Syafiqah Habdul Latif[1], Sheikh Ahmad Izaddin Sheikh Mohd Ghazali[1], Erna Normaya Abdullah[2], Azizul Hakim Lahuri[3], Mohammad Fadzlee Ngatiman[4], and Nur Nadia Dzulkifli[1*]

[1]Faculty of Applied Sciences, Universiti Teknologi MARA Negeri Sembilan Branch, Kuala Pilah Campus, 72000 Negeri Sembilan, Malaysia

[2]Experimental and Theoretical Research Laboratory, Department of Chemistry, Kulliyah of Science, International Islamic University Malaysia, Bandar Indera Mahkota, 25200 Kuantan, Pahang, Malaysia

[3]Department of Basic Science and Engineering, Faculty of Agriculture and Food Sciences, Universiti Putra Malaysia Bintulu, 97008 Sarawak, Malaysia

[4]Center for Research and Instrumentation Management (CRIM), Universiti Kebangsaan Malaysia, 43600 Bangi, Selangor, Malaysia

Received March 12, 2018; Accepted August 1, 2018

ABSTRACT

Corrosion of metal is a serious issue across many industries and is considered costly. Acids used during the cleaning process in industries may contribute to metal erosion. Dithiocarbamate is a ligand that can act as a corrosion inhibitor due to the presence of sulfur and nitrogen as electronegative atoms. Zn(II) N-*isopropylbenzyldithiocarbamate (Zn[*N-*isopbenzdtc]$_2$) complex was synthesized through direct synthetic method of < 4 °C and characterized using Fourier Transform Infrared-Attenuated Total Reflectance (FTIR-ATR), Ultraviolet-Visible (UV-Vis), Nuclear Magnetic Resonance (NMR), X-ray crystallography study, molar conductivity, melting point, and gravimetric analysis. Corrosion inhibition of mild steel was studied for different corrosive media (1 M HCl and 1 M H_2SO_4). The synthesized inhibitor was studied at different concentrations of 1, 2, 3, 4, and 5 mM at 40 °C. As a conclusion, as the inhibitor concentration decreased, the efficiency of the corrosion inhibitor also decreased at a constant temperature. In this study, it showed that the corrosion activity of mild steel in 1 M H_2SO_4 was higher compared to 1 M HCl due to the higher concentration of H^+, which makes H_2SO_4 more corrosive than HCl.*

Keywords: *dithiocarbamate; corrosion inhibitor; mild steel; acid*

ABSTRAK

Korosi logam merupakan masalah serius di banyak industri dan dianggap mahal. Asam yang digunakan selama proses pembersihan dalam industri dapat menyebabkan erosi logam. Ditiokarbamat adalah ligan yang dapat bertindak sebagai inhibitor korosi karena kehadiran sulfur dan nitrogen sebagai atom elektronegatif. Zn(II) N-*isopropilbenzilditiokarbamat (Zn [*N-*isopbenzdtc]$_2$) kompleks disintesis melalui metode sintetik langsung < 4 °C dan dikarakterisasi menggunakan Fourier Transform Infrared-Attenuated Total Reflectance (FTIR-ATR), Ultraviolet-Visible (UV-Vis), Nuclear Magnetic Resonance (NMR), studi kristalografi sinar-X, konduktivitas molar, titik leleh, dan analisis gravimetri. Penghambatan korosi baja ringan dipelajari untuk media korosif yang berbeda (1 M HCl dan 1 M H_2SO_4). Inhibitor yang disintesis dipelajari pada konsentrasi yang berbeda dari 1, 2, 3, 4, dan 5 mM pada 40 °C. Sebagai kesimpulan, ketika konsentrasi inhibitor menurun, efisiensi inhibitor korosi juga menurun pada suhu konstan. Dalam penelitian ini, menunjukkan bahwa aktivitas korosi baja ringan dalam 1 M H_2SO_4 lebih tinggi dibandingkan dengan 1 M HCl karena konsentrasi H^+ yang lebih tinggi, yang membuat H_2SO_4 lebih korosif daripada HCl.*

Kata Kunci: *ditiokarbamat; inhibitor korosi; baja ringan; asam*

INTRODUCTION

Acids are normally used for the removal of undesirable scale and rust in metalwork, especially in chemical cleaning process [1]. Dithiocarbamates are sulfur-nitrogen containing ligands that possess a diversity of coordination chemistry. Dithiocarbamate is a flexible class of monoanionic 1,1-dithio ligand which

* Corresponding author.
Email address : nurnadia@ns.uitm.edu.my

DOI: 10.22146/ijc.34703

molds a stable compound that displays a diversity of coordination modes either with transition or non-transition metal ions [2]. In previous studies, metal dithiocarbamate complexes have been recognized as compounds that are widely studied in different fields. Dithiocarbamate in the definition of inorganic chemistry is known as a flexible ligand with its ability to chelate with numerous types of metal ions [3]. The possession of two donor sulfur atoms that exist in the ligand greatly influences the chelating properties of dithiocarbamate [3]. Heterocyclic organic compounds are competent corrosion inhibitors used to prevent the corrosion of mild steel due to the π system [4].

Mirzakhanzadeh et al., reported zinc aluminum polyphosphate (ZAPP) as a corrosion inhibitor. This corrosion inhibition provided by zinc aluminum polyphosphate on a mild steel due to the formation of a protective layer and bound the contact of the corrosive agent to resurface on the steel apparent [5]. Phosphate-based pigments are known as a non-toxic inorganic inhibitor that is widely used for the shield of various metals [5]. The corrosion inhibition mechanism of polyphosphates lay about the existence of high phosphate content and its chelate building potential with zinc metal cation [5]. Meanwhile, the application of zinc ferrocyanide ion exchange compounds was acknowledged as inhibiting and sensing pigments in protective paints and primers for metals and alloys [6]. The inhibition routine of zinc ferrocyanide in the coating was inspected by salt spray tests [6]. The work suggests that zinc ferrocyanide can discharge the inhibitors at enough rate to inhibit the corrosion of aluminium alloys in aggressive salt spray tests [6]. In comparison with this new research on zinc dithiocarbamate, the corrosion inhibition evaluation was performed with weight loss analysis in acid by using mild steel. Throughout the study, zinc has been known as a strong cathodic inhibitor of localized corrosion.

Dithiocarbamate has various applications for industrial which one of them is applied as a corrosion inhibitor. Typically, zinc is used as a protective coating in the galvanization process to avert rust and erosion of metals such as iron. Zinc coating provides protection against a steel exterior that prevents oxygen and moisture from interacting with the steel surface, which can lead to deterioration. Corrosion is a serious environmental issue in the industrial sector [7]. The effectiveness of the inhibitor against corrosion was studied on mild steel. Mild steel was used in trials for corrosion analysis. Mild steel is one of the essential engineering materials due to its low cost and also has excellent mechanical properties that are broadly used as a construction material in the industries [8]. The use of mild steel as a construction material in the industrial sector has become a challenge for corrosion engineers or scientists these days. Mild steel is severely attacked by acid solutions that are used in various industries. Acid inhibitors are frequently used in order to reduce corrosion dependent or independent attack by an acid on metals [9]. This inhibitor produced due to the corrosion problem in industrial. An acid used during the cleaning process lead to metal corrosion. Therefore, this research aimed at the synthesis of an eco-environmental friendly corrosion inhibitor based on zinc by an in-situ method. The effectiveness of dithiocarbamate inhibitor determined by a using weight loss method where a mild steel immersed in the absence and presence of inhibitor in an acidic environment. For this research, Dithiocarbamate inhibitor was cast-off for industrial by adding it into an acid that used for the metal cleaning process. Hence, the aims of this study were synthesized, characterization, and anticorrosion screening of Zn(II) *N*-isopropylbenzyldithiocarbamate (Zn[*N*-isopbenzdtc]$_2$) complex on a mild steel with different acids. Besides, the chemical properties of the title compound were studied using density functional theory (DFT) calculation. Anti-corrosion inhibitor is the most fitting product to avert the corrosion problem when it comes to metal corrosion inhibition. It is able to provide a good lubrication and long-term prevention to the metals which exposed to rust and corrosion. This anti-corrosion inhibitor breaches and coats the metal surfaces and gives the rust protection.

EXPERIMENTAL SECTION

General Methods

The melting point of the synthesized complex was determined in an open capillary tube with an electrothermal melting point apparatus (SMP10 Stuart). The value of molar conductivity of the complex was measured with dimethylformamide (DMF) solvent at room temperature using Lab 970 conductivity meter (SI Analytics) at the concentration of 1×10^{-3} M. The percentage of metal was determined by gravimetric analysis. The electronic spectra were measured by a spectrophotometer (T80/80+, PG Instruments) in the region of 200–600 cm^{-1}. The infrared spectra of the compounds were verified within the spectral range of 4000–650 cm^{-1} using Perkin Elmer model GX spectrophotometer. ^{1}H and ^{13}C NMR spectra of dithiocarbamate complex were recorded in dimethyl sulfoxide (DMSO) solution at room temperature and the chemical shifts were given in ppm (σ scale). X-ray crystallography study was executed on a Bruker Apex II CCD diffractometer at 0 K. The structural and bonding properties of the complex were studied using DFT calculations.

Chemical Synthesis

Synthesis of Zn(II) dithiocarbamate complex, Zn[N-isopbenzdtc]$_2$

The ratios of amine, carbon disulfide (CS_2), and salt were 2:2:1, respectively. 2 mmol of *N*-isopropylbenzyl amine was stirred in a conical flask for 30 min at < 4 °C. A cold methanolic solution of 2 mmol of CS_2 was added to the flask containing the previous solution. The mixture was stirred for another 30 min. Multiple drops of ammonia were mixed continuously into the solution while the pH of the solution was maintained at a range of 6–7 and the stirring was resumed for another 1 h. After 1 h, a methanolic solution of 1 mmol Zn(II) chloride was added to the mixture with continuous stirring for another 2 h. A precipitate started to form throughout 2 h of stirring. Next, the precipitate was filtered and rinsed with methanol. After that, the precipitate was dried overnight in an oven at 70 °C. The purity of the precipitate was checked using Thin Layer Chromatography (TLC) plate. The precipitate was recrystallized by methanol to obtain a single crystal suitable for analysis by X-ray crystallography.

Corrosion Inhibition Study

Preparation of acids and different concentrations of inhibitor

1 M HCl and 1 M H_2SO_4 were prepared using the formula $M_1V_1 = M_2V_2$. The acid was diluted in a 250 mL volumetric flask. Different concentrations of inhibitor were set at 1, 2, 3, 4, and 5 mM.

Weight Loss Analysis

Mild steels with the dimension of 2 cm × 2 cm were selected to be tested for weight loss analysis. The mild steels were cut into rectangular sheets. The mild steels were scraped by emery paper and washed with distilled water, followed by acetone, and dried with clean tissue paper. After that, the initial weights of mild steels were measured using an analytical balance. The mild steels were then immersed in 10 mL of 1 M HCl for different inhibitor concentrations of 1, 2, 3, 4, and 5 mM for about 24 h. Then, the mild steels were rinsed with distilled water, followed by acetone, and dried with clean tissue paper. The mild steels were reweighed to compare the final weight after immersion with the initial weight before immersion to determine the weight loss that reflected the corrosion rate. Weight loss was determined in the presence and absence of inhibitors at 40 °C and at different inhibitor concentrations. The procedures were repeated using another acid, 1 M H_2SO_4, with same concentrations and a constant temperature of 40 °C.

Computational Method

The crystal structure was optimized in solution phase using a continuum solvent model (CPCM) by a B3LYP/LANL2DZ basis set and further study was continued to calculate the chemical properties of the title compound using the Gaussian 09 software. The GaussView 5.0 program was used to construct the highest occupied molecular orbital (HOMO), lowest unoccupied molecular orbital (LUMO) energy distributions, and molecular electrostatic potential [10-11].

RESULT AND DISCUSSION

Physical Measurements

The in-situ method was used for the synthesis of Zn[*N*-isopbenzdtc]$_2$ in which the ligand is the intermediate of the complete synthesis. The synthesis was performed by the reaction of carbon disulfide (CS_2), amine (*N*-isopropylbenzylamine), and salt (Zn(II) chloride). The white-colored precipitate was observed, indicating the complete synthesis of the complex. The percentages of carbon, nitrogen, hydrogen, and sulfur were determined using an elemental analyzer for Zn[*N*-isopbenzdtc]$_2$. Table 1 shows the percentages of the elements in Zn[*N*-isopbenzdtc]$_2$. Fig. 1 shows the proposed structure of the synthesized inhibitor. The melting point recorded for the complex was 144 °C. The molar conductivity measurement recorded was 15 µS/cm. Zn[*N*-isopbenzdtc]$_2$ complex is categorized as a non-electrolyte where the non-electrolyte behavior shows that the complex does not contain any counterion and the ligand is directly coordinated to the metal center.

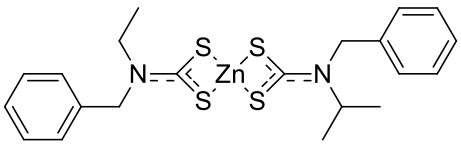

Fig 1. The proposed structure of Zn[*N*-isopbenzdtc]$_2$

Table 1. The percentage of the element of Zn[*N*-isopbenzdtc]$_2$

Complex	Color	% Y	M (℃)	Elemental analysis (calculated)			
				C	H	N	S
Zn[*N*-isopbenzdtc]$_2$	Colorless	82	144	51.38 (51.40)	5.40 (5.49)	5.42 (5.45)	24.78 (24.95)

% Y; percentage yield, M (°C); melting points

Table 2. Electronic spectra data for Zn[*N*-isopbenzdtc]$_2$ and raw materials

Compounds	Transition	λmax (nm)	Molar absorptivity, ε (M^{-1} cm^{-1})
Carbon disulphide, CS2	n→σ*	210	66900
N-isopropylbenzylamine	n→σ*	225	94000
	n→σ*	250	70000
	π→π*	290	15400
Zn[N-isopbenzdtc]2	n→σ*	230	25700
	n→σ*	260	66800
	π→π*	284	36400

Table 3. Selected FTIR-ATR absorption for starting materials and Zn[*N*-isopbenzdtc]$_2$, cm^{-1}

Compound	Wavenumber, cm^{-1}					
	v(C-H)	*v*(N-H)	*v*(C=S)	*v*(C⎓S)	*v*(C-N)	*v*(C⎓N)
Carbon disulphide, CS_2	-	-	1497	-	-	-
N-isopropyl Benzylamine	2966	3448	-	-	1453	-
Zn[*N*-isopbenzdtc]$_2$	2972	-	-	1413	1452	1472

The calculated percentage of the analyte, Zn(II) obtained from the gravimetric analysis was 12.72%.

Ultraviolet-Visible (UV-Vis)

Table 2 represents the electronic spectra data for the complex and raw materials. The n→σ* transition of CS_2 was recorded at 210 nm and for *N*-isopropylbenzylamine, the transitions were recorded at 225 and 250 nm. Meanwhile, for Zn[*N*-isopbenzdtc]$_2$, the n→σ* transitions were observed at 230 and 260 nm. The absorption peaks at 205 to 280 nm were identified as the intraligand transition due to n→σ*, whereas the absorption peaks around 280 to 355 nm were also recognized as the intraligand transition due to π→π* [12]. The existence of n→σ* transition showed the presence of sulfur and nitrogen atoms [13]. Besides, the π→π* transition also appeared in *N*-isopropylbenzylamine at 290 nm. Meanwhile, the π→π* transition for Zn[*N*-isopbenzdtc]$_2$ was verified at 284 nm peak with molar absorptivity, ε, recorded at 36400 M^{-1} cm^{-1}. By comparing between the amine and the synthesized inhibitor, the π→π* transition moved downward, which showed higher energy for the complex. The complex undergoes a hypsochromic shift, which is a shift of a spectral band to higher energy with a shorter wavelength due to the coordination of the metal [14]. There is an absence of n→π* transition because the transition is Laporte forbidden, which is a weak absorption. No absorption occurred at a range higher than 400 nm, which represents the *d*-*d* transition because Zinc (d^{10}) is full of electrons in the *d* orbital.

Fourier Transform Infrared-Attenuated Total Reflectance

The stretching band of v(C-N) was 1453 cm^{-1} for *N*-isopropylbenzylamine. Meanwhile, v(C-N) for the synthesized complex was 1452 cm^{-1}. According to [15], the v(C⎓N) appeared at 1470-1500 cm^{-1} is assigned as a thioureide band. The complex showed a new stretching band, v(C⎓N) at 1472 cm^{-1} due to its partial double-bond character, where there was partial delocalization of π-electron density within dithiocarbamate [16]. The band appeared at greater wavenumber due to the delocalization of electrons toward the center metal after being coordinated with dithiocarbamate ligands [17]. The region of v(C=S) of CS_2 was observed at the peak of 1497 cm^{-1} while for Zn[*N*-isopbenzdtc]$_2$, the band of v(C⎓S) was observed at 1413 cm^{-1}. This condition has proven that for the structure of Zn(II) complex, the stretching band shifted to lower wavenumber due to the decrease of carbon-sulfur double-bond character to partial double-bond character. The stretching band of v(N-H) disappeared at the complex after the hydrogen from amine has been deprotonated by ammonia as tabulated in Table 3. The infrared absorption spectrum of the metal dithiocarbamate complex has been acknowledged as a vital element in order to allocate the coordination mode, either monodentate or bidentate dithiocarbamate ligands. The v(C⎓S) band was detected at 1012 cm^{-1}, which designated the bidentate chelating mode of the ligand coordinated towards the metal cation [18]. As a whole, the existence of only one band in the 1000 ± 70 cm^{-1} region is due to the bidentate character, while the splitting of the same band in the same region is due to the monodentate character [19]. The bidentate chelating mode of Zn[*N*-isopbenzdtc]$_2$ has been affirmed with the appearance of a single peak at 1063 cm^{-1}.

Nuclear Magnetic Resonance

The ^{1}H NMR spectrum of Zn[*N*-isopbenzdtc]$_2$ displayed a doublet at 1.095–1.112 ppm corresponding to methyl proton (–CH_3). The CH proton attached to the nitrogen still appeared upfield due to its proton integration corresponding which is more shielded [20].

Table 4. ^{1}H NMR and ^{13}C NMR of Zn[*N*-isopbenzdtc]$_2$ complex

Complex	Signal position (δ, ppm)	Compound	Structure
^{1}H NMR	1.095-1.112 (a)	-CH_3	
	3.332 (b)	-CH	
	5.118 (c)	-CH_2	
	5.281-5.331 (h)	-CH	
	7.221-7.365 (d, e, f, g)	-CH (benzene)	
^{13}C NMR	20.44 (a)	-CH_3	
	51.51 (b)	-CH	
	56.27 (c)	-CH_2	
	126.93, 127.15 (g)	-CH (benzene)	
	128.65-129.22 (e,f)	-CH (benzene)	
	138.06 (d)	-CH (benzene)	
	206.14 (h)	-C=S	

Table 5. Crystal data and structure refinement for Zn[*N*-isopbenzdtc]$_2$

Empirical formula	C_{22} H_{28} N_2 S_4 Zn
Formula weight	514.07
Temperature	293(2) K
Wavelength	0.71076 Å
Crystal system	Orthorhombic
Space group	$P2_12_12_1$
Unit cell dimensions	*a* = 9.044(8) Å *a*= 90°. *b* = 11.464(10) Å *b*= 90°. *c* = 24.36(2) Å *γ* = 90°.
Volume	2525(4) Å^3
Z	4
Density (calculated)	1.352 Mg/m^3
Absorption coefficient	1.314 mm^{-1}
F(000)	1072
Crystal size	0.470 x 0.460 x 0.310 mm^3
Theta range for data collection	2.988 to 28.338°.
Index ranges	-12<=h<=12, -15<=k<=13, -32<=l<=32
Reflections collected	39026
Independent reflections	6264 [R(int) = 0.1167]
Completeness to theta = 25.243°	99.8 %
Refinement method	Full-matrix least-squares on F^2
Data / restraints / parameters	6264 / 0 / 266
Goodness-of-fit on F^2	1.083
Final R indices [I>2sigma(I)]	R1 = 0.0695, wR2 = 0.1694
R indices (all data)	R1 = 0.1068, wR2 = 0.1937

The ^{1}H NMR CH (b) proton was found at the region of 3.332 ppm while CH (h) at 5.281–5.331 ppm. CH_2 appeared at the region of 5.118 ppm. The presence of nitrogen atom causes the hydrogen attached to the carbon to be deshielded downfield. Based on [13], the nitrogen atom is attracted toward the carbon atom due to its electron-drawing effect and this reduces the electron density of the proton attached to the carbon. The region at 7.221–7.365 ppm indicates the CH proton of the benzene ring. The transition is the deshielding factor of the anisotropy of the ring and the resonance that steals electron density of nitrogen while alters its hybridization [13]. The ^{13}C NMR spectrum of Zn[*N*-isopbenzdtc]$_2$ is also compatible with its structure as stated in Table 4. There were seven peaks in ^{13}C NMR, which means that the amount of carbon in Zn[*N*-isopbenzdtc]$_2$ was symmetric. The first peak of ^{13}C NMR was observed at 20.44 ppm, which showed the transition of CH_3 carbon. ^{13}C chemical shifts of thioureide carbon atoms are associated with the π bonding in NCS_2^-. Meanwhile, the methyl carbons, CH and CH_2 in Zn[*N*-isopbenzdtc]$_2$ were deshielded due to the bonding with the nitrogen of thioureide π system and the signals were detected at 51.51 and 56.27 ppm, respectively. The compounds with carbon-carbon double bonds or aromatic rings contribute to the increase of chemical shifts in the range from 100 to 175 ppm [13]. The

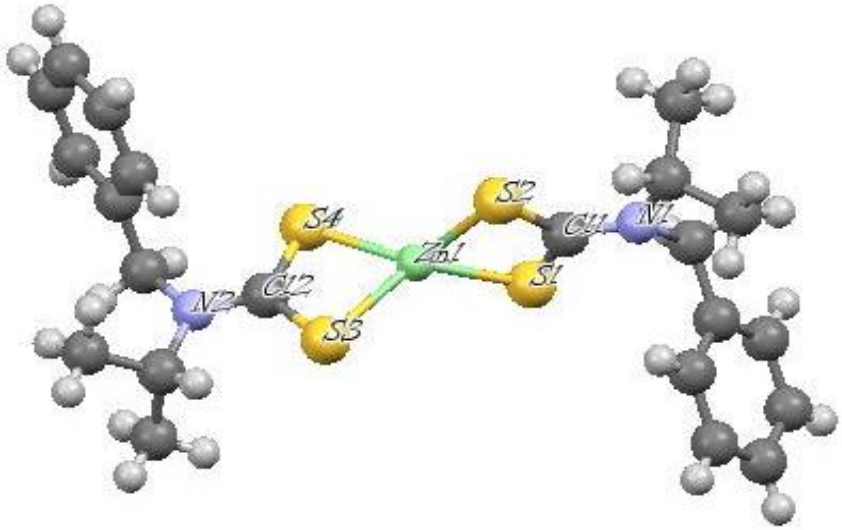

Fig 2. Crystal structure of Zn[*N*-isopbenzdtc]$_2$ complex

Table 6. Bond lengths [Å] and angles [°] for Zn[*N*-isopbenzdtc]$_2$

Bond lengths [Å]			
Zn(1)-S(1)	2.324(3)	S(1)-C(11)	1.728(8)
Zn(1)-S(3)	2.332(3)	S(2)-C(11)	1.739(7)
Zn(1)-S(2)	2.342(3)	S(3)-C(12)	1.730(8)
Zn(1)-S(4)	2.344(2)	S(4)-C(12)	1.726(7)
N(1)-C(11)	1.306(9)	N(2)-C(12)	1.312(9)
N(1)-C(7)	1.473(9)	N(2)-C(16)	1.459(11)
N(1)-C(8)	1.492(11)	N(2)-C(13)	1.486(11)
Bond angles [°]			
S(1)-Zn(1)-S(3)	131.88(9)	C(11)-S(1)-Zn(1)	83.1(2)
S(1)-Zn(1)-S(2)	78.25(7)	C(11)-S(2)-Zn(1)	82.4(3)
S(3)-Zn(1)-S(2)	119.36(10)	C(12)-S(3)-Zn(1)	82.9(2)
S(1)-Zn(1)-S(4)	125.05(10)	C(12)-S(4)-Zn(1)	82.6(2)
S(3)-Zn(1)-S(4)	77.89(9)	C(11)-N(1)-C(7)	120.0(6)
S(2)-Zn(1)-S(4)	132.64(9)	C(11)-N(1)-C(8)	121.1(6)
C(12)-N(2)-C(16)	121.1(7)	C(7)-N(1)-C(8)	117.9(6)
C(12)-N(2)-C(13)	120.3(7)	C(16)-N(2)-C(13)	118.5(6)

benzene ring showed three peaks in the aromatic carbon area of a proton-decoupled ^{13}C spectrum since ortho and meta carbon are symmetric, where the spectrum appeared at 128.65 to 129.22 ppm. Meanwhile, para carbon aromatic ring was recorded at 126.93 to 127.15 ppm. The singlet arose from CH carbon of benzene ring that has no attached hydrogen appeared at 138.07 ppm. Benzylic carbon is deshielded by the anisotropic field of the ring created by π electrons in the ring system, but the distance is getting further from the ring, which results in a smaller effect [13]. The spectrum at 206.14 ppm was defined as C=S peak as the carbon is deshielded due to the attachment to a sulfur atom that acts as an electronegative atom. The carbon attached to the double bond is also deshielded due to diamagnetic anisotropy [13].

X-Ray Crystallographic Study

The synthesized complex was crystallized in an orthorhombic crystal system with a space group of a = 9.044 (8) Å, $P2_12_12_1$. The crystallographic data are summarized in Table 5. Selected bond lengths and angles of the complex are listed in Table 6. The crystal of Zn[*N*-isopbenzdtc]$_2$ compound adopts a distorted tetrahedral geometry as shown in Fig. 2. The metal atom Zn was coordinated to four sulfur atoms with the bond angles of S(1)–Zn(1)–S(2), S(1)–Zn(1)–S(3), S(1)–Zn(1)–S(4), S(2)–Zn(1)–S(3), S(2)–Zn(1)–S(4), and S(3)–Zn(1)–S(4), which correspond to 78.25, 131.87, 125.05, 119.35, 132.64, and 77.89°, respectively. Zn(1)-S(3)-S(4)-C(12) moiety was twisted (79.73°) with respect to Zn(1)-S(1)-S(2)-C(11) plane. Meanwhile,

Table 7. Corrosion inhibition data of Zn[*N*-isopbenzdtc]$_2$ in 1 M HCl

Inhibitor	Inhibitor concentrations (mM)	Weight loss, ΔW (g)	Corrosion rate, C_{RW} (g cm^{-2} h^{-1})	Inhibitor efficiency, η_w (%)
Blank	1000 (1 M)	0.186	1.9375 x 10^{-3}	-
Zn[*N*-isopbenzdtc]$_2$	1	0.153	1.5938 x 10^{-3}	17.74
	2	0.131	1.3646 x 10^{-3}	29.57
	3	0.115	1.1979 x 10^{-3}	38.17
	4	0.104	1.0833 x 10^{-3}	44.09
	5	0.100	1.0417 x 10^{-3}	46.23

Table 8. Corrosion inhibition data of Zn[*N*-isopbenzdtc]$_2$ in 1 M H_2SO_4

Inhibitor	Inhibitor concentrations (mM)	Weight loss, ΔW (g)	Corrosion rate, C_{RW} (g cm^{-2} h^{-1})	Inhibitor efficiency, η_w (%)
Blank	1000 (1 M)	0.429	4.4688 x 10^{-3}	-
Zn[*N*-isopbenzdtc]$_2$	1	0.362	3.7708 x 10^{-3}	15.62
	2	0.309	3.2188 x 10^{-3}	27.97
	3	0.274	2.8542 x 10^{-3}	36.13
	4	0.251	2.6146 x 10^{-3}	41.49
	5	0.238	2.4792 x 10^{-3}	44.52

S(3)-S(4)-C(12) moiety was twisted (116.5° [4]) from S(2)-S(1)-C(11), which was 116.3° [4]. The bond angles were slightly different from the ideal bond angle for tetrahedral geometry, which was 109.5° [21]. The structure constriction leads to the alteration in the coordination of metal ion as compared to an ideal geometry [22]. A large divergence in the metal to S_{short} with the metal to S_{long} bond distances is attributed to the coordinating features of the metal dithiocarbamate complex [23]. The bidentate features of the synthesized complex are also characterized by a large difference in C-S bond length: S(1)–C(11) = 1.7281 Å, S(2)–C(11) = 1.7392 Å, S(3)–C(12) = 1.7298 Å, and S(4)–C(12) = 1.7261 Å. The presence of thioureide bond in the synthesized complex was also verified in X-ray crystallography study, which is consistent with the infrared result [23]. According to [24], the C⋯S bond length is shorter than the C-S single bond length of 1.81 Å and longer than the C=S bond length of 1.69 Å, which are suggestive of partial double-bond properties. The thioureide length of N(1)–C(11) = 1.3064 Å and N(2)–C(12) = 1.3119 Å suggests that the molecule contains the partial double-bond character as compared to the normal C-N and C=N bond length of 1.47 Å and 1.28 Å, correspondingly [25]. The short thioureide bond length compared to the normal bond distance of C-N is due to the delocalization of π-electron density over S_2CN moiety.

Corrosion Inhibition Study

The effect of the addition of synthesized inhibitor at different concentrations on the corrosion of mild steel in 1 M HCl and 1 M H_2SO_4 was studied using weight loss method at 40 °C after 24 h immersion [26]. Different concentrations of synthesized inhibitor were also studied in acidic media of 1, 2, 3, 4, and 5 mM. Table 7 and 8 present the influence of different concentrations of the inhibitor on inhibition efficiency in 1 M HCl and 1 M H_2SO_4, respectively. The calculated values of η_w of the synthesized inhibitor indicated that η_w increased with increasing inhibitor concentration, with a maximum η_w of Zn[*N*-isopbenzdtc]$_2$ in 1 M HCl of 46.23%. The inhibitory action of the inhibitor was determined as the adsorption on the mild steel surface and able to form an opaque protective layer, which was found to increase with the increasing concentration of the inhibitor [27]. Meanwhile, in 1 M H_2SO_4, there was a maximum η_w of 44.52% using 5 mM inhibitor concentration. The corrosion inhibition of Zn[*N*-isopbenzdtc]$_2$ in 1 M HCl and 1 M H_2SO_4 can be explained through the adsorption of respective molecules on the exterior of mild steel [26]. The adsorption of the inhibitor on the mild steel surface creates a blockage for mass and charge transfer and accordingly, mild steel is protected from hostile acid solution [26]. Fig. 3 shows the graph of a comparison of corrosion activity between 1 M HCl and 1 M H_2SO_4. The corrosion activity in H_2SO_4 was higher than HCl, where the corrosion rate in H_2SO_4 was greater compared to HCl, as shown in Fig. 4. This is because the presence of high concentrations of H^+ in H_2SO_4 makes the acid more corrosive compared to HCl [28]. H_2SO_4 is highly corrosive as emphasized by its highly exothermic (generates heat) reaction with water [29]. The formula for corrosion rate, C_{RW} and inhibitor efficiency, η_w is shown in Eq. (1).

$$\Delta W = W_1 - W_2 \quad (1)$$

$$C_{RW} = \frac{\Delta W}{s \times t} \quad (2)$$

$$\theta = \frac{C^\circ_{RW} - C_{RW}}{C^\circ_{RW}} \quad (3)$$

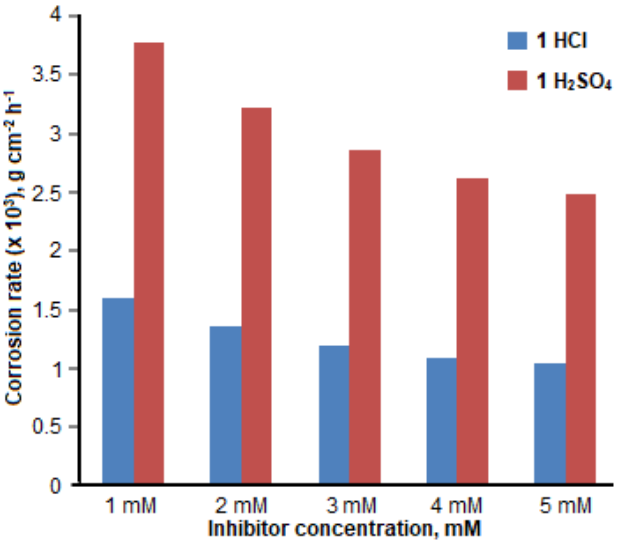

Fig 3. Graph of inhibitor concentration versus corrosion rate between 1 M HCl and 1 M H_2SO_4

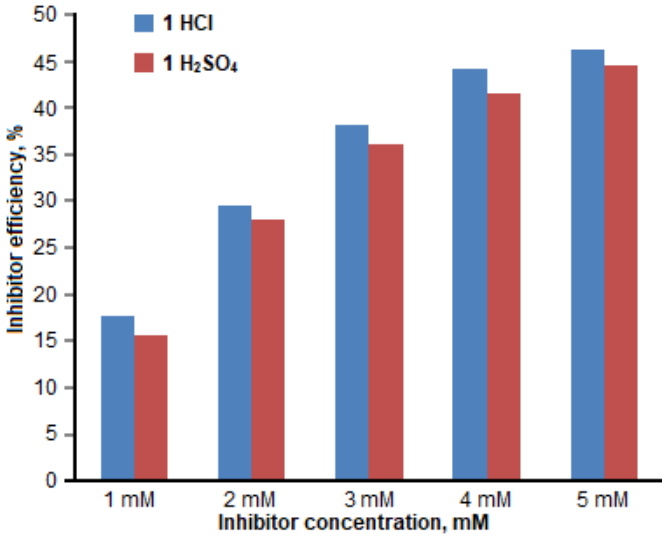

Fig 4. Graph of inhibitor concentration versus inhibitor efficiency between 1 M HCl and 1 M H_2SO_4

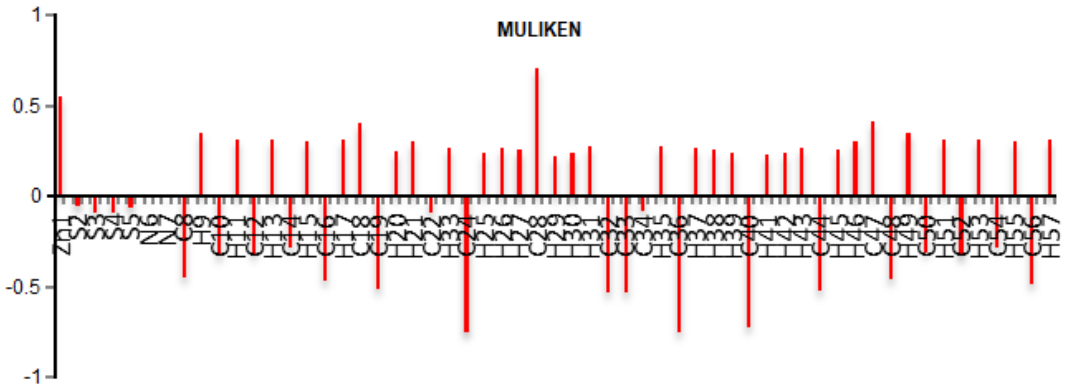

Fig 5. Bar diagram representing the charge distribution of the Zn[*N*-isopbenzdtc]$_2$

$$n_w = \frac{C°_{RW} - C_{RW}}{C°_{RW}} \times 100\% \quad (4)$$

where,

W_1 = The initial weight of mild steel before immersion (g); W_2 = The final weight of mild steel after immersion (g); ΔW = The weight loss (g); s = The surface area of the mild steel (cm); T=Time of immersion (h); C_{RW} = The corrosion rate in the presence of inhibitor (g cm^{-2} h^{-1}); $C°_{RW}$ = The corrosion rate in the absence of inhibitor (g cm^{-2} h^{-1}); η_w=The percentage of inhibitor efficiency (%).

Chemical Properties Study

Atomic charge analysis

The charge distribution of the molecule was calculated on the basis of Mulliken method using B3LYP/6-311++G(d,p) level calculations. This calculation represents the charges of every atom in the molecule. Mulliken population analysis computes charges by dividing the orbital overlap evenly between the two atoms involved [30]. As shown in Fig. 5, the atoms that exhibit positive charges are Zn1, H9, H11, H13, H15, H17, C18, H20, H21, H33, H25, H26, H27, C28, H29, H30, H31, H35, H37, H38, H39, H41, H42, H43, H45, H46, C47, H45, H46, H49, H51, H53, H55, and H57, whereas S2, S3, S4, N6, N7, C8, C10, C12, C14, C16, C19, C22, C24, C32, C34, C36, C40, C44, C48, C50, C52, C54, and C56 exhibit negative charges. All hydrogen atoms possess positive charges. The bar diagram also shows that the negative charges of S atoms decreased due to the complex formation.

Chemical reactivity properties

Chemical reactivity properties can be evaluated by calculating Frontier Molecular Orbital (FMO) energies. The results are listed in Table 9. The negative formation energy showed that the complex formed was thermodynamically stable with value -1061.241 eV. The value of the dipole moment is related to the corrosion inhibitor property. The dipole moment of the title complex

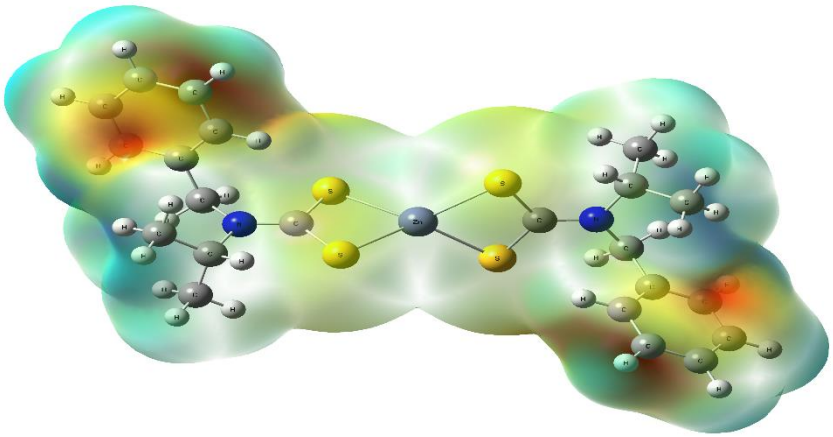

Fig 6. The molecular electrostatic potential (MEP) of the Zn[*N*-isopbenzdtc]$_2$

Table 9. The calculated chemical reactivity properties of the Zn[*N*-isopbenzdtc]$_2$

Chemical Properties	Value
Energy	-1070.672362 eV
Dipole moment	0.3289 Debye
Ionization energy	-7.09455595 eV
Electron affinity	-4.9405016 eV

was 1.1829 Debye, showed that the compound was polarizable and act effectively as a corrosion inhibitor in this study. Theoretical study of ionization energy and affinity electron involved to the chemical inertness and stability of the compound. Higher ionization energy is needed to ensure the stability of the compound to act as a corrosion inhibitor. The calculation showed that the ionization and the affinity electron of the title complex are 6.8975 and 4.9780 eV, respectively. These theoretical results also were supported by experiments that showed the complex ability to act effectively as a corrosion inhibitor.

Molecular electrostatic potential

Molecular electrostatic potential (MEP) of the title compound is illustrated in Fig. 6. MEP is widely used as a reactivity map displaying the regions for electrophilic and nucleophilic attacks [31-33]. As can be seen from the figure, the most electronegative atoms in this complex are S atoms, which have pale yellow color. This situation showed that S atoms had donated their electron and formed a coordinate bond with Zn in the complex formation.

CONCLUSION

In conclusion, by using the in-situ method, Zn[*N*-isopbenzdtc]$_2$ complexes have been successfully synthesized, which gave sharp melting point and characterized by FTIR-ATR, NMR, UV-Vis, gravimetric analysis, molar conductivity, and X-ray single-crystal diffraction. The structure of the synthesized complex revealed that the coordination in the complex is S,S-bidentate coordination. The NMR and IR spectra were in full agreement with X-ray single-crystal diffraction. The crystal structure of Zn[*N*-isopbenzdtc]$_2$ complex adopts a distorted tetrahedral geometry, which is coordinated to thiolate sulfur of ligand. The chemical properties such as the energy of complex formation, dipole moment, ionization energy, and electron affinity of the title complex have been successfully calculated using DFT approach. The theoretical study through charge analysis and molecular electrostatic potential also showed that the electron density of electronegative sulfur atoms decreased after the formation of the title complex. The weight loss analysis of mild steel revealed a result in as the inhibitor concentration is increased, the efficiency of the inhibitor also increased in which the maximum inhibitor efficiency recorded. The inhibitor efficiency in 1 M H_2SO_4 is lower compared to 1 M HCl as the increase of inhibitor concentration. It is because of the presence of high concentrations of H^+ in H_2SO_4 which makes it more corrosive compared to HCl.

ACKNOWLEDGEMENT

This work was supported by the research grant from the Ministry of Higher Education with the grant number of FRGS/1/2016/STG01/UITM/03/6. We are grateful to everyone involved in this project. We would also like to express our gratitude to the Faculty of Applied Sciences, Universiti Teknologi MARA (UiTM) Negeri Sembilan Branch, Kuala Pilah Campus, Negeri Sembilan Darul Khusus, Malaysia and the Centre of Research and Instrumentation Management (CRIM), Universiti Kebangsaan Malaysia, Selangor Darul Ehsan, Malaysia for providing facilities used in this work.

REFERENCES

[1] Obi-Egbedi, N.O., and Obot, I.B., 2013, Xanthione: A new and effective corrosion inhibitor for mild steel in sulphuric acid solution, *Arabian J. Chem*., 6 (2), 211–223.

[2] Dar, S.H., Thirumaran, S., and Selvanayagam, S., 2015, Synthesis, spectral and X-ray structural studies on Hg(II) dithiocarbamate complexes: A new precursor for HgS nanoparticles, *Polyhedron*, 96, 16–24.

[3] Kamaludin, N.F., Awang, N., Baba, I., Hamid, A., and Meng, C.K., 2013, Synthesis, characterization and crystal structure of organotin(IV) *N*-butyl-*N*-phenyldithiocarbamate compounds and their cytotoxicity in human leukemia cell lines, *Pak. J. Biol. Sci*., 16 (1), 12–21.

[4] Karthikaiselvi, R., and Subhashini, S., 2012, The water soluble composite poly(vinylpyrrolidone-methylaniline): A new class of corrosion inhibitors of mild steel in hydrochloric acid media, *Arabian J. Chem*., 10, 627–635.

[5] Mirzakhanzadeh, Z., Kosari, A., Moayed, M.H., Naderi, R., Taheri, P., and Mol, J.M.C., 2018, Enhanced corrosion protection of mild steel by the synergetic effect of zinc aluminum polyphosphate and 2-mercaptobenzimidazole inhibitors incorporated in epoxy-polyamide coatings, *Corros. Sci*., 138, 372–379.

[6] Li, J., and Buchheit, R., 2016, Development of zinc ferrocyanide ion exchange compounds for corrosion-inhibiting and sensing pigments, *Prog. Org. Coat*., 104, 210–216.

[7] Srimathi, M., Rajalakshmi, R., and Subhashini, S., 2014, Polyvinyl alcohol–sulphanilic acid water soluble composite as corrosion inhibitor for mild steel in hydrochloric acid medium, *Arabian J. Chem*., 7 (5), 647–656.

[8] Ansari, K.R., and Quraishi, M.A., 2014, Bis-schiff bases of isatin as new and environmentally benign corrosion inhibitor for mild steel, *J. Ind. Eng. Chem*., 20 (5), 2819–2829.

[9] Hussin, M.H., Jain Kassim, M., Razali, N.N., Dahon, N.H., and Nasshorudin, D., 2016, The effect of *Tinospora crispa* extracts as a natural mild steel corrosion inhibitor in 1 M HCl solution, *Arabian J. Chem*., 9, 616–624.

[10] Frisch, A., Nielsen, A.B., Holder, A.J., 2001, *GaussView User Manual*, Gaussian, Inc., Pittsburgh.

[11] Frisch, M.J., Trucks, G.W., Schlegel, H.B., Scuseria, G.E., Robb, M.A., Cheeseman, J.R., Scalmani, G., Barone, V., Petersson, G.A., Nakatsuji, H., Li, X., Caricato, M., Marenich, A., Bloino, J., Janesko, B.G., Gomperts, R., Mennucci, B., Hratchian, H.P., Ortiz, J.V., Izmaylov, A.F., Sonnenberg, J.L., Williams-Young, D., Ding, F., Lipparini, F., Egidi, F., Goings, J., Peng, B., Petrone, A., Henderson, T., Ranasinghe, D., Zakrzewski, V.G., Gao, J., Rega, N., Zheng, G., Liang, W., Hada, M., Ehara, M., Toyota, K., Fukuda, R., Hasegawa, J., Ishida, M., Nakajima, T., Honda, Y., Kitao, O., Nakai, H., Vreven, T., Throssell, K., Montgomery, J.A., Peralta Jr., A.E., Ogliaro, F., Bearpark, M., Heyd, J.J., Brothers, E., Kudin, K.N., Staroverov, V.N., Keith, T., Kobayashi, R., Normand, J., Raghavachari, K., Rendell, A., Burant, J.C., Iyengar, J., Tomasi, S.S., Cossi, M., Millam, J.M., Klene, M., Adamo, C., Cammi, R., Ochterski, J.W., Martin, R.L., Morokuma, K., Farkas, O., Foresman, J.B., and Fox, D.J., 2009, *Gaussian 09, Revision E.01,* Gaussian, Inc., Wallingford.

[12] Onwudiwe, D.C., Nthwane, Y.B., Ekennia, A.C., and Hosten, E., 2016, Synthesis, characterization and antimicrobial properties of some mixed ligand complexes of Zn(II) dithiocarbamate with different *N*-donor ligands, *Inorg. Chim. Acta*, 447, 134–141.

[13] Pavia, D.L., Lampman, G.M., Kriz, G.S., and Vyvyan, J.R., 2015, *Introduction to Spectroscopy*, 5th ed., Cengage Learning Asia, Singapore, 624.

[14] Abou-Hussein, A.A., and Linert, W., 2015, Synthesis, spectroscopic studies and inhibitory activity against bacteria and fungi of acyclic and macrocyclic transition metal complexes containing a triamine coumarine schiff base ligand, *Spectrochim. Acta, Part A*, 141, 223–232.

[15] Mutalib, A.F.A., Baba, I., Farina, Y., and Samsudin, M.W., 2011, Synthesis and characterization of diphenyltin(IV) dithiocarbamate compounds, *MJAS*, 15 (1), 106–112.

[16] Reyes-Martínez, R., Mejia-Huicochea, R., Guerrero-Alvarez, J.A., Höpfl, H., and Tlahuext, H., 2008, Synthesis, heteronuclear NMR and X-ray crystallographic studies of two dinuclear diorganotin(IV) dithiocarbamate macrocycles, *ARKIVOC*, 5, 19–30.

[17] Ajibade, P.A., and Ejelonu, B.C., 2013, Group 12 dithocarbamate complexes: Synthesis, spectral studies and their use as precursors for metal sulfides nanoparticles and nano composites, *Spectrochim. Acta, Part A*, 113, 408–414.

[18] Tamilvanan, S., Gurumoorthy, G., Thirumaran, S., and Ciattini, S., 2017, Synthesis, characterization, cytotoxicity and antimicrobial studies on Bi(III) dithiocarbamate complexes containing furfuryl group and their use for the preparation of Bi_2O_3 nanoparticles, *Polyhedron*, 121, 70–79.

[19] Abdullah, N.H., Zainal, Z., Silong, S., Tahir, M.I.M., Tan, K.B., and Chang, S.K., 2016, Synthesis of zinc sulphide nanoparticles from thermal decomposition

of zinc *N*-ethyl cyclohexyl dithiocarbamate complex, *Mater. Chem. Phys*., 173, 33–41.

[20] Sivasekar, S., Ramalingam, K., Rizzoli, C., and Alexander, N., 2014, Synthesis, structural, continuous shape measure and bond valence sum characterization of bismuth(III) complexes of substituted dithiocarbamates and their solvothermal decomposition, *Inorg. Chim. Acta*, 419, 82–88.

[21] Khan, N., Farina, Y., Mun, L.K., Rajab, N.F., and Awang, N., 2014, Syntheses, spectral characterization, X-ray studies and *in vitro* cytotoxic activities of triorganotin(IV) derivatives of *p*-substituted *N*-methylbenzylaminedithiocarbamates, *J. Mol. Struct*., 1076, 403–410.

[22] Naqeebullah, Farina, Y., Chan, K.M., Mun, L.K., Rajab, N.F., and Ooi, T.C., 2013, Diorganotin(IV) derivatives of *N*-methyl *p*-fluorobenzo-hydroxamic acid: Preparation, spectral characterization, X-ray diffraction studies and antitumor activity, *Molecules*, 18 (4), 8696–8711.

[23] Kamaludin, N.F., and Awang, N., 2014, Synthesis and characterisation of organotin(IV) *N*-ethyl-*N*-phenyldithiocarbamate compounds and the crystal structures of dibutyl- and triphenyltin(IV) *N*-ethyl-*N*-phenyldithiocarbamate, *Res. J. Chem*. *Environ*., 18 (11), 99–107.

[24] Sonia, A.S., and Bhaskaran, R., 2017, Tris dithiocarbamate of Co(III) complexes: Synthesis, characterization, thermal decomposition studies and experimental and theoretical studies on their crystal structures, *J. Mol. Struct*., 1134, 416–425.

[25] Halimehjani, A.Z., Torabi, S., Amani, V., Notash, B., and Saidi, M.R., 2015, Synthesis and characterization of metal dithiocarbamate derivatives of [3-((pyridin-2-yl)methylamino)propanenitrile]: Crystal structure of [3-((pyridin-2-yl)methylamino) propanenitriledithio-carbamato] nickel(II), *Polyhedron*, 102 (2), 643–648.

[26] Zarrouk, A., Zarrok, H., Ramli, Y., Bouachrine, M., Hammouti, B., Sahibed-dine, A., and Bentiss, F., 2016, Inhibitive properties, adsorption and theoretical study of 3,7-dimethyl-1-(prop-2-yn-1-yl)quinoxalin-2(1H)-one as efficient corrosion inhibitor for carbon steel in hydrochloric acid solution, *J. Mol. Liq*., 222, 239–252.

[27] Olajire, A.A., 2017, Corrosion inhibition of offshore oil and gas production facilities using organic compound inhibitors-a review, *J. Mol. Liq*., 248, 775–808.

[28] Samina, M., Karim, A., and Venkatachalam, A., 2011, Corrosion study of iron and copper metals and brass alloy in different medium, *E-J. Chem*., 8, 344–349.

[29] van der Hagen, M., and Järnberg, J., 2009, *140. Sulphuric, Hydrochloric, Nitric and Phosphoric Acids*, The Nordic Expert Group for Criteria Documentation of Health Risks from Chemicals, vol. 43, Torén, K., eds., Sahlgrenska Academy, University of Göteborgs, Sweden, 81–96.

[30] Sidir, I., Sidir, Y.G., Kumalar, M., and Tasal, E., 2010, Ab initio Hartree–Fock and density functional theory investigations on the conformational stability, molecular structure and vibrational spectra of 7-acetoxy-6-(2,3-dibromopropyl)-4,8-dimethyl coumarin molecule, *J. Mol. Struct*., 964 (1-3), 134–151.

[31] Luque, F.J., Lopez, J.M., and Orozco, M., 2000, Perspective on "Electrostatic interactions of a solute with a continuum. A direct utilization of ab initio molecular potentials for the prevision of solvent effects", *Theor. Chem. Acc*., 103, 343–345.

[32] Okulik, N., and Jubert, A.H., 2005, Theoretical analysis of the reactive sites of non-steroidal anti-inflammatory drugs, *Internet electron. J. Mol. Des*., 4 (1), 17–30.

[33] Parlak, C., Akgogan, M., Yildirim, G., Karagoz, N., Budak, E., and Terzioglu, C., 2011, Density functional theory study on the identification of 3-[(2-morpholinoethylimino) methyl]benzene-1,2-diol, *Spectrochim. Acta, Part A*, 79 (1), 263–271.